

0017-9310(95)00390-8

Natural convection in a cubical cavity heated from below at low Rayleigh numbers

J. PALLARÈS, I. CUESTA,† F. X. GRAU and FRANCESC GIRALT*

Departament d'Enginyeria Elèctrica i Mecànica, *Departament d'Enginyeria Química,
Escola Tècnica Superior d'Enginyeria Química, Universitat Rovira i Virgili,
Ctra. Salou s/n, 43006 Tarragona, Spain

(Received 17 May 1995 and in final form 15 September 1995)

Abstract—Natural convection in a cubical cavity heated from below is examined by means of the three-dimensional computation of the time dependent Navier–Stokes and energy transport equations in the range of Rayleigh numbers $3500 \leq Ra \leq 10\,000$. The Boussinesq approximation has been used to model buoyancy effects on momentum transfer. Four different stable convective structures occur with orientation and flow circulation dictated by the combined effect of the four adiabatic confining lateral walls. Three of these structures are typical single rolls with their axis of rotation or vorticity horizontal and either parallel to two opposite vertical walls, structures S1 and S3, or orientated towards two opposite vertical edges (S2). The fourth structure (S4) is a nearly toroidal roll with the descending motion aligned with the four vertical edges and the single ascending current along the vertical axis of the enclosure. The effect of the Rayleigh number and the type of flow structure on heat transfer rates at the top and bottom plates is also reported. For the single roll-type structures the surface averaged Nusselt number increases with a power of the Rayleigh number that changes within the range studied from 0.7 to 0.4. A similar trend is observed for the toroidal roll but in this case heat transfer rates are 65% lower. The distribution of local heat transfer coefficients at the top and bottom surfaces agrees with the topology of the flow patterns portrayed with the aid of the second invariant of the velocity gradient and the modulus of the cross product of the corresponding velocity and vorticity fields. Copyright © 1996 Elsevier Science Ltd.

INTRODUCTION

Natural convection is a fundamental mechanism for momentum, heat and mass transfer in some natural phenomena and of interest in engineering systems. Independently from its geophysical, meteorological, astrophysical and engineering applications, natural convection in enclosures heated from below has been the topic of numerous theoretical and experimental studies because of its geometric simplicity and fundamental implications. Among all possible configurations, the cubical cavity offers the additional interest of not having any preferred direction other than the direction of gravity. This characteristic enables the occurrence of different complex flow structures under steady-state conditions for a given set of Rayleigh and Prandtl numbers. Furthermore, each structure affects the transfer of heat from the hot to the cold plate differently and the average Nusselt number becomes a function of the Rayleigh and Prandtl numbers and of the type of structure present.

The Rayleigh–Bénard convection (RB) problem [1] in cavities has been extensively studied theoretically, experimentally and numerically since the beginning of the present century [2, 3]. Koschmieder [4], Normand *et al.* [5], Oertel [6], Ostrach [7] and Yang [8] defined and described the main characteristics of the flow in

heated enclosures. Flow stability is mainly affected by fluid properties, enclosure geometry and the external field. It is well known that there is a critical Rayleigh number (Ra_c) for RB convection beyond which a buoyancy-driven flow develops with a corresponding increase in transfer rates. In the cubical cavity with lateral adiabatic walls the critical Rayleigh number is 3446 [9]. This theoretical value agrees with the experimental work of Heitz and Westwater [10]. On the other hand, RB convection in a cubical cavity with perfectly conducting lateral walls presents a critical Rayleigh number of 7000 [11, 12].

Concerning the topology of the flow, Ozoe *et al.* [13] obtained two convective structures in the supercritical region $4000 \leq Ra \leq 8000$ for the cubical cavity with adiabatic lateral walls. Both patterns may be described as single circulating rolls, one with axis parallel to two opposite vertical walls and the other with axis parallel to the diagonal of the horizontal walls. Recently Hernández and Frederick [14] found numerically a new convective structure at $Ra = 8000$ which exhibits a characteristic toroidal like form, with flow descending near the four vertical edges and ascending at the central vertical axis of the cube.

The purpose of this study is to characterize numerically the natural convection in a cubical cavity where buoyancy has been induced by imposing a moderate temperature difference between the bottom (hot) and the top (cold) plates with perfectly adiabatic vertical

† Author to whom correspondence should be addressed.

NOMENCLATURE

g	gravitational acceleration [m s^{-2}]	Greek letters	
H	$ \mathbf{H} \times \boldsymbol{\omega} $ [m s^{-2}]	α	thermal diffusivity [$\text{m}^2 \text{s}^{-1}$]
L	reference length [m]	β	thermal expansion coefficient [K^{-1}]
n	normal dimensionless coordinate	δ_{ij}	Kronecker delta
N	number of grid nodes in one direction	ν	kinematic viscosity [$\text{m}^2 \text{s}^{-1}$]
Nu	Nusselt number, hL/k	Π	second invariant of the velocity gradient tensor [s^{-2}]
P	pressure [Pa]	$\boldsymbol{\omega}$	vorticity vector [s^{-1}]
Pr	Prandtl number, ν/α	$\boldsymbol{\Omega}_{ij}$	rotation tensor, $\boldsymbol{\Omega}_{ij}\boldsymbol{\Omega}_{ji} = -\boldsymbol{\omega}^2/2$ [s^{-2}]
Ra	Rayleigh number, $g\beta\Delta TL^3/\nu\alpha$	Δ	increment.
Ra_c	critical Rayleigh number	Superscripts and subscripts	
S_{ii}	strain tensor [s^{-1}]	s	surface averaged quantity
T	temperature [K]	*	dimensionless quantity
\mathbf{U}	velocity vector [m s^{-1}]	c	cold wall
u, v, w	velocity components [m s^{-1}]	h	hot wall
x, y, z	Cartesian coordinates [m].	o	average quantity.

walls. The occurrence and topology of the different types of stable convective structures are examined within the interval $3500 \leq Ra \leq 10000$ and their effect in heat transfer rates at the top and bottom plates is characterized. Flow and heat transfer for the two roll-typed structures previously described by Ozoe *et al.* [13] with a coarser grid, hereinafter referred to as S1 and S2, are determined. The occurrence of an additional new roll-type structure (S3) with different topological and heat transport features is also reported. Finally, the flow and heat transfer characteristics of the toroidal roll (S4) described by Hernández and Frederick [14] at $Ra = 8000$ and a 21^3 grid, is determined at $Ra = 9000$ and 10000 using a finer 41^3 grid.

GOVERNING EQUATIONS

The geometry of the cubical cavity and the coordinate system is shown in Fig. 1. Both the bottom and the top plates are taken to be isothermal with the lower one held at temperature T_h which is moderately greater than the temperature of the upper wall T_c . The four vertical walls are perfectly insulated.

The fluid considered in this study is air ($Pr = 0.71$). Compressibility effects, viscous dissipation and the

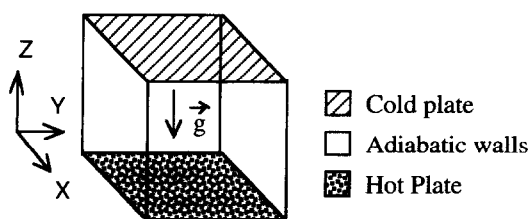


Fig. 1. Physical model of the cubical cavity heated from below.

variation of fluid properties with temperature have been neglected, with the only exception of the buoyancy term, for which the Boussinesq approximation has been adopted. As a result, the Navier–Stokes and the energy transport equations are coupled only by the body force term, where linear dependence of density with temperature is assumed. According to Gray and Giorgini [15], the Boussinesq approximation for air at mean temperature $T_o = 15^\circ\text{C}$ and $P = 1$ atm, holds for temperature differences up to 28.6°C when the two horizontal walls are 1 m apart.

The reference scales for length, velocity, time and pressure are, respectively, L , α/L , L^2/α and $\rho\alpha^2/L^2$. The non-dimensional temperature is defined as

$$T^* = \frac{T - T_o}{\Delta T} = \frac{T - (T_h + T_c)/2}{T_h - T_c} \quad (1)$$

while all other variables are converted into dimensionless form using the above scales. The non-dimensional governing transport equations in Cartesian coordinates are,

$$\frac{\partial u_i^*}{\partial x_j^*} = 0 \quad (2)$$

for continuity,

$$\frac{\partial u_i^*}{\partial t^*} + \frac{\partial (u_j^* u_i^*)}{\partial x_j^*} = -\frac{\partial P^*}{\partial x_i^*} + Pr \frac{\partial^2 u_i^*}{\partial x_j^* \partial x_j^*} + Ra Pr T^* \delta_{i3} \quad (3)$$

for momentum and

$$\frac{\partial T^*}{\partial t^*} + \frac{\partial (u_j^* T^*)}{\partial x_j^*} = \frac{\partial^2 T^*}{\partial x_j^* \partial x_j^*} \quad (4)$$

for energy.

NUMERICAL METHOD

Numerical scheme

The CFD code 3DINAMICS [16, 17] was used to obtain numerical solutions of the above governing equations with second order accuracy and in terms of the primitive variables. In this code equations (2)–(4) are discretized following a control volume scheme [18] with non-uniform three-dimensional staggered grids. All computational grids used in the present study were regular. The convective fluxes across the surfaces of the control volumes were discretized using a second order QUICK scheme [19]. 3DINAMICS incorporates the non-uniform grid version of QUICK proposed by Perng and Street [20] to enhance convergence. Second order approximations were also implemented for the diffusive fluxes with a centered scheme. The SMAC algorithm [21] was applied to compute the pressure field. This algorithm is based on a typical predictor–corrector scheme and leads to a fractional step method for the velocity–pressure coupling.

A critical step in the pressure algorithm, that affects the global performance of the code, is the solution of the Poisson equation. According to Koshla and Rubin [22] a much faster solution of Poisson-like equations is obtained with the Conjugate Gradient Method than with other methods. This methodology has been adopted in the present study. Convergence was increased by using the diagonal scaling technique to precondition the coefficient matrix. A semi-implicit, second order accurate, ADI method [23] was applied for time-marching integration.

Heat transfer rates at the top and bottom walls is characterized with local and surface averaged Nusselt numbers defined, respectively, by

$$Nu = \left. \frac{\partial T^*}{\partial z^*} \right|_{z^*=0 \text{ or } 1} \quad (5)$$

and

$$Nu_S = \int_0^1 \int_0^1 Nu \, dx^* \, dy^* \quad (6)$$

Equations (5) and (6) were solved using second order finite differences and interpolation schemes.

The boundary conditions for the dynamic field are $u_i = 0$ at the walls, i.e., all six walls of the cavity are assumed to be rigid and at rest. The thermal boundary conditions are $(\partial T / \partial n) = 0$ at the four adiabatic vertical walls, $T_B^* = 0.5$ at bottom plate and $T_C^* = -0.5$ at the top plate.

Even though the RB problem with air in a cubical enclosure at Rayleigh numbers below 10 000 has only steady solutions, the numerical simulations using 3DINAMICS provide a complete description of the time-evolution towards steady-state conditions.

As initial conditions, the fluid was assumed to be at rest and a conductive temperature distribution was established in the whole domain. In order to enhance

the RB convective regime, a random disturbance in the temperature field with an amplitude of ± 0.05 (10% of the local temperature) was added to this initial thermal field [24]. This strategy avoids the pre-determination of the final convective structure. All four structures described in this work have been obtained starting all computations from this unbiased initial condition at different Rayleigh numbers. The use of other initial conditions, such as a non-uniform heating or cooling at the bottom or top plates, respectively, or a non-adiabatic condition at any of the four lateral walls during a short computational time, could favour the development of any of the aforementioned four structures, as well as that of other convective motions not reported in the present study for the range of Rayleigh numbers covered. Results obtained at a given Rayleigh number were successively used as initial conditions for computations at higher or lower Rayleigh numbers, to check the stability of the structures.

Validation

Cuesta [16] and Cuesta *et al.* [17] validated 3DINAMICS describing the flow in a cubical cavity driven either by the upper moving lid or the simultaneous heating and cooling of two opposite vertical walls. Among these computations, the natural convection results are of special relevance to the present work. As it can be seen in Table 1, heat transfer rates predicted by Cuesta *et al.* [17] for two lateral and opposite walls in the range $10^3 \leq Ra \leq 10^6$ are in good agreement with numerical predictions reported elsewhere [25–28].

The performance of 3DINAMICS in the RB problem is established by comparing predictions with other numerical results and experimental data, and by verifying the grid-independence of the present results. First, present results are consistent with previous computations, namely those of Ozoe *et al.* [13] and Hernández and Frederick [14]. Table 2 shows predicted Nusselt numbers for the structures S1 and S4 at different values of the Rayleigh number. It should be noted that Ozoe *et al.* [13] reported two different structures of the flow, S1 and S2, but only provided heat transfer rates for structure S1. There is good agreement between present and previous predictions with discrepancies being caused by differences in grid size and Prandtl number.

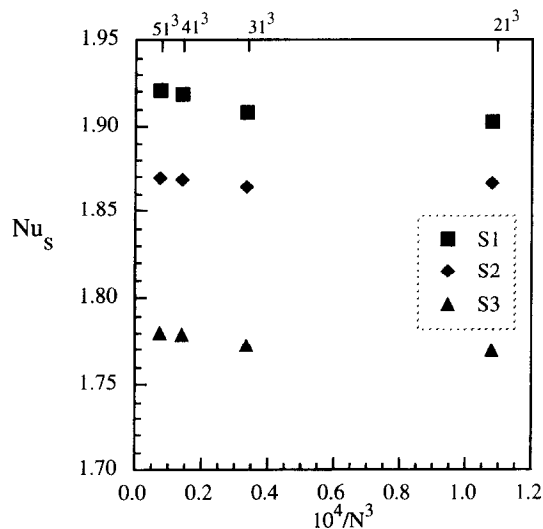
The grid independence study was carried out at $Ra = 10\,000$. Starting with the coarsest grid of 21^3 control volumes, the grids were successively refined to 31^3 , 41^3 and 51^3 with uniformly distributed nodes. Figure 2 shows the evolution of the predicted surface averaged Nusselt number with the inverse of the number of grid points for the three single roll-typed structures S1–S3 reported in this study. Structure S4 can only be obtained at $Ra\ 10\,000$ with the finest grids of 41^3 and 51^3 nodes. It should be noted that at this Rayleigh number this structure is close to a new transition and the influence of the boundary layer at the

Table 1. Comparison between several surface averaged Nusselt numbers reported in the literature for the side-heated cubical cavity

Ra	Cuesta [16] 3D	Fusegi <i>et al.</i> [25] 3D	Haldenwang [26] 3D	B. Mabrouk [27] 3D	David-Jones [28] 2D
10^3	1.052	1.085	-	1.073	1.118
10^4	2.187	2.1	-	2.083	2.243
10^5	4.512	4.361	4.31	4.452	4.519
10^6	8.846	8.77	8.61	9.215	8.8

Table 2. Comparison between several surface averaged Nusselt numbers reported in the literature for the cubical cavity heated from below

Author	Ra	Pr	Structure	Nu_s	Nu_s present work
Ozoe <i>et al.</i> [13]	4000	1	S1	1.165 (9 ³)	1.164 (41 ³)
	6000	1	S1	1.535 (9 ³)	1.522 (41 ³)
	8000	1	S1	1.746 (9 ³)	1.755 (41 ³)
Hernández and Frederick [14]	8000	0.71	S4	1.1 (21 ³)	1.04 (41 ³) 1.06 (21 ³)

Fig. 2. Surface averaged Nusselt number for the convective structures S1, S2 and S3 at $Ra = 10\,000$ for different grid densities.

lateral walls can only be captured with these finest grids. According to Fig. 2, increasing the nodes from 41^3 to 51^3 does not represent more than 0.3% variation in terms of the surface averaged Nusselt number. A similar discrepancy has been obtained for S4. According to these results, the regular mesh of 41^3 points was used in all the computations.

To our knowledge, only numerical results are available in the literature for cubical cavities. In order to

check 3DINAMICS with experimental results, those obtained by Arroyo and Savirón [29] for Rayleigh number 11 000 and Prandtl number 130, at an average temperature of 25°C, have been selected. The physical dimensions of the cavity used by Arroyo and Savirón [29] are $L_x = 25$ mm, $L_y = 14.6$ mm and $L_z = 12.3$ mm, with silicon oil ($Pr = 130$) as working fluid. Figure 3 shows the comparison between these data and present predictions, in terms of isoline of either constant u -velocity or constant w -velocity, at the central ($y = \text{constant}$) plane, where v -velocity equals zero. The numerical results obtained with a regular grid of $41 \times 21 \times 21$ nodes are in good agreement qualitatively and quantitatively with the experimental data. Note that this grid is coarser in the x and z directions than the 41^3 used in the present calculations for the cubical cavity.

RESULTS AND DISCUSSION

Visualization

The visualization of three-dimensional (3D) dynamic fields is still a challenge in CFD, mainly because of their vectorial character. The objective of such visualization is to portray an image of the flow structure. The most common approach is to plot vector fields or, similarly, fields of streamlines, pathlines or streaklines, all coincident in steady-state regimes. The definition of stream surfaces is somehow ambiguous because there are infinite ways of connecting streamlines. Despite this fact, this technique is one of the most suitable ways to 'freeze' a 3D flow field [30].

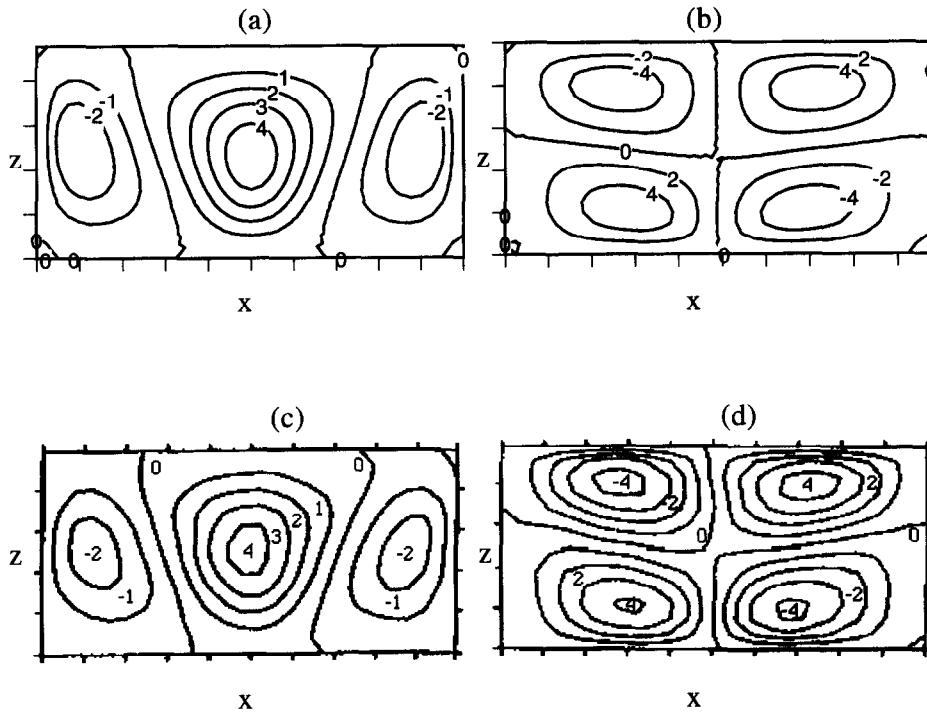


Fig. 3. Isovelocity component maps for w , (a) and (c): $\Delta w = 44.9 \mu\text{m s}^{-1}$, and u , (b) and (d): $\Delta u = 30.6 \mu\text{m s}^{-1}$ at $Ra = 11\,000$ ($Pr = 130$). (a) and (b) Numerical solutions; (c) and (d) experimental data of Arroyo and Savirón [29].

Usually, secondary magnitudes such as pressure, the modulus of vorticity or the enstrophy (the square of vorticity) are used to explore and identify flow structures in a dynamic field. These variables, however, take finite but usually large values at the walls, which can interfere and lead to a misinterpretation of the structure present in the flow. An alternative is to use a passive contaminant, such as temperature in an uncoupled dynamic field, to mark any structure present. This technique has the problem of diffusion which can smear the picture of a flow structure, specially at the edges. Also, it is difficult to establish initial conditions for this thermal field. In fact, the use of a passive contaminant with zero diffusivity is the basis of the method described by van Wijk *et al.* [30] for plotting stream surfaces.

In additions to particle tracking and plotting surfaces of constant temperature we have explored, in this work, two alternative magnitudes to describe the structural characteristics of the flow: the second invariant of the velocity gradient tensor, hereinafter called Π , and the modulus of the vector product of the velocity and the vorticity, hereinafter called H . In non-dimensional form, these quantities are defined, respectively, by

$$H^* = |\mathbf{U}^* \times \boldsymbol{\omega}^*| \quad (7)$$

and

$$\Pi^* = \frac{\partial u_i^*}{\partial x_j^*} \frac{\partial u_j^*}{\partial x_i^*} = \mathbf{S}_{ij}^* \mathbf{S}_{ji}^* + \boldsymbol{\Omega}_{ij}^* \boldsymbol{\Omega}_{ji}^* \quad (8)$$

The second invariant Π has already been used to identify structures in turbulent flows [31, 32], because regions of space with negative values of Π coincide with regions where rotation prevails over strain. The variable H is related to helicity [33], the scalar product of vorticity and velocity

$$H^2 = |\mathbf{U}|^2 \boldsymbol{\omega}^2 - (\mathbf{U} \times \boldsymbol{\omega})^2 \quad (9)$$

and has the property of emphasizing regions of relatively high vorticity and velocity without falling to zero in two dimensional flows, as is the case with helicity.

Figures 4 and 5 show the isosurfaces of Π and H , respectively, for the three structures obtained at $Ra = 4000$ (S1–S3). Figures 6 and 7 depict the same isosurfaces for the four structures (S1–S4) present at $Ra = 9000$. Figures 4 and 5 include some particle paths to illustrate that the fluid circulates around the closed surfaces with large negative values of Π .

Dynamic field

The dynamic fields plotted in Figs. 4–7 indicate that structures S1 and S3 are formed by single rolling motions with clockwise or anti-clockwise rotation. The axis of rotation of the roll is parallel to the coor-

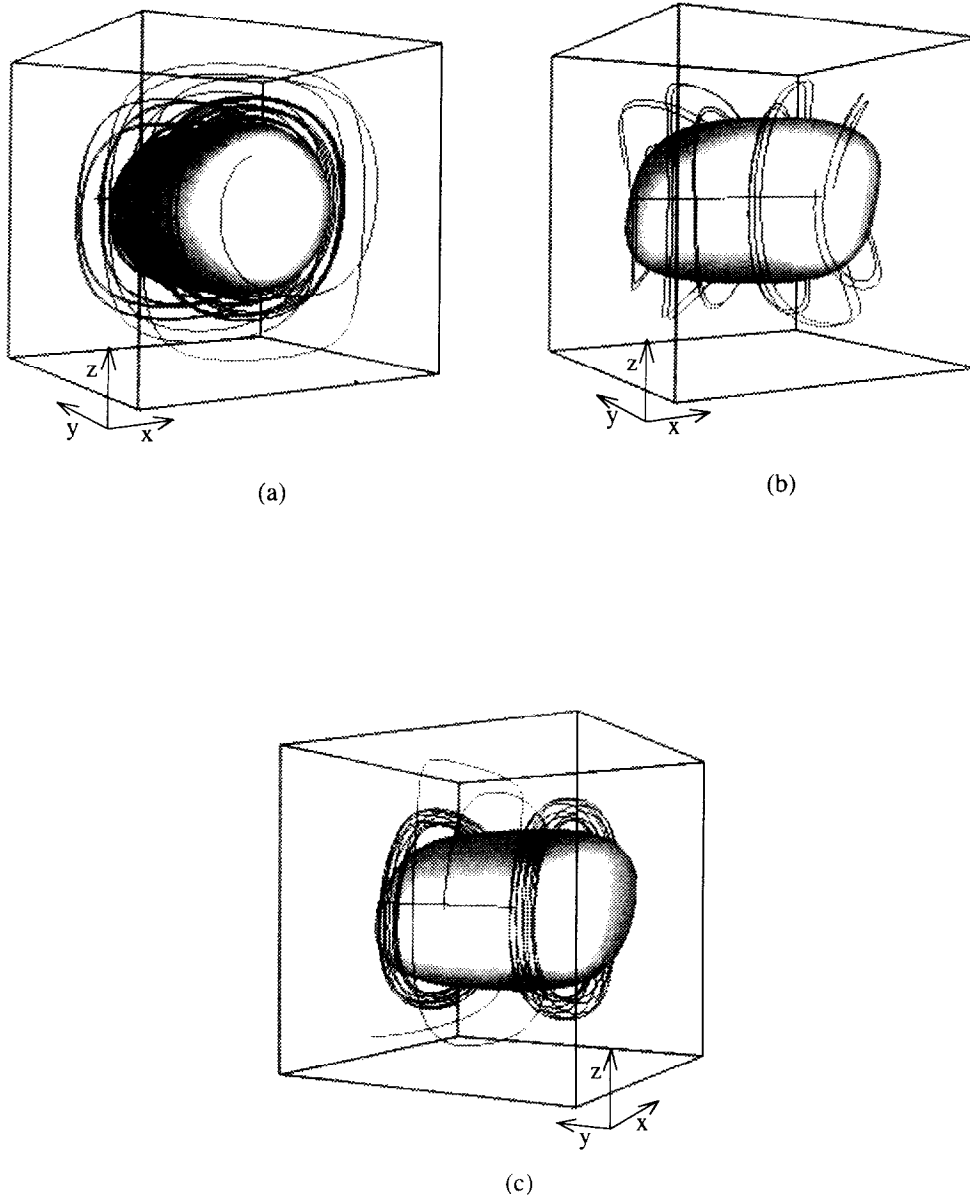


Fig. 4. Isosurfaces of the second invariant of the velocity gradient tensor at $Ra = 4000$ for the structures S1 (a) $\Pi^* = -250$; S2 (b) $\Pi^* = -200$; (c) $\Pi^* = -190$.

dinate x or y , indistinctly. These two possible orientations are equivalent due to the symmetry of the enclosure. Their sense of rotation depends only on the random thermal distribution mentioned before. Increasing the Rayleigh number produces an elongation of the S1 and S3 roll towards the two opposite top and bottom edges that are parallel to the axis of rotation and towards which the structure is tilted. There is a great similarity between S1 and S3 but some differences are revealed when comparing Figs. 4(a)

and (c) or 5(a) and (c). The structure S3 is more tilted and elongated towards the top and bottom opposite edges than S1. This fact produces a substantial difference in the heat transfer rates for both structures at the top and bottom plates, as it is discussed in the next section.

The second structure (S2) is also a single roll but with a diagonal mode of circulation. It shows a greater three-dimensionality than S1 and S3 and the flow is strongly affected by the increase of the Rayleigh

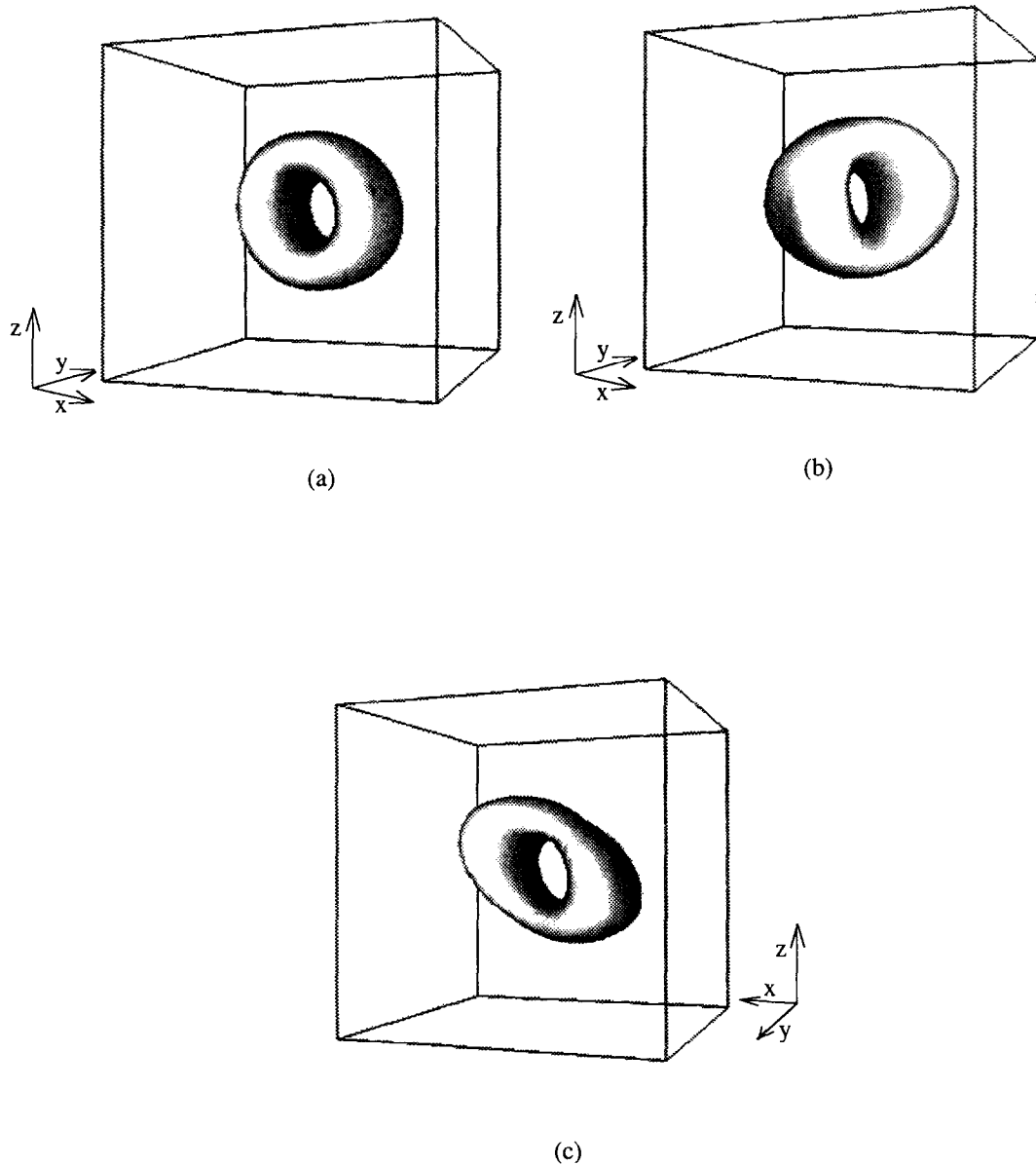


Fig. 5. Isosurfaces of the cross product modulus at $Ra = 4000$ for the structures S1 (a) $H^* = 175$; S2 (b) $H^* = 130$; S3 (c) $H^* = 130$.

number. Comparison of the isosurfaces of the second invariant for S2 at $Ra = 4000$ and at $Ra = 9000$, Figs. 4(b) and 6(b), shows that the flow in the regions near the corners of the cubical cavity is clearly modified. The structure is somehow 'twisted' towards the four opposite corners at the highest Rayleigh number. The particle traces also reveal this change.

The critical Rayleigh number for the three roll structures S1–S3 is about 3500, in agreement with the theoretical prediction of Catton [9] and the experimental work of Heitz and Westwater [10].

The structure S4 has been found to exist only for Rayleigh numbers equal to or above 8000. Present heat transfer results (Fig. 11) suggest an approximate critical Rayleigh number of 7700. The topology of S4 over the range of Rayleigh numbers studied is characterized by a cold descending current in the central region of the enclosure. Heating of this current at the bottom plate while moving towards the four lower corners causes the fluid to ascend parallel to the vertical edges and to close the recirculation pattern depicted in Figs 6(d) and 7(d) in terms of Π and H .

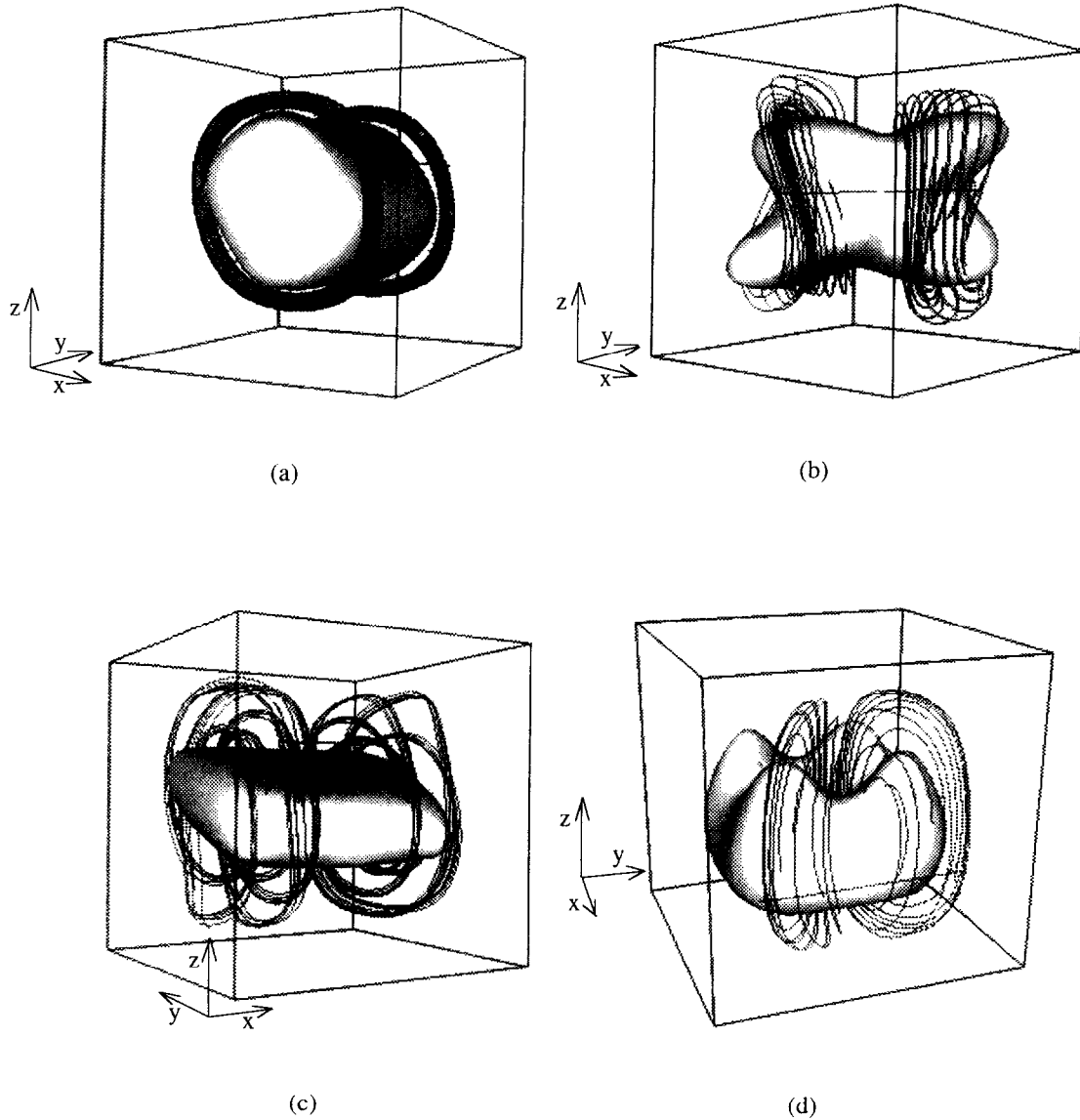


Fig. 6. Isosurfaces of the second invariant velocity gradient tensor at $Ra = 9000$ for the structures S1 (a) $\Pi^* = -3000$; S2 (b) $\Pi^* = -4000$; S3 (c) $\Pi^* = -3000$; S4 (d) $\Pi^* = -500$.

respectively. It is also feasible to simulate numerically the reverse flow pattern, i.e. ascending hot fluid at the core and descending at the vertical edges, depending on the initial conditions used.

Figure 8 depicts the flow pattern of S4 at $Ra = 8000$ in terms of the velocity field at the 2D plane $X^* = 0.5$. This method of visualization has been the most widely used in the literature to analyse vector fields [34], because it provides the direct representation of the direction and magnitude of vectors at discrete locations. Figure 8 shows that the projection of the velocity field on the vertical plane $X^* = 0.5$ is in good agreement with the corresponding maps reported by

Hernández and Frederick [14] for this structure. Inspection of this figure clearly shows that a single roll with toroidal shape occurs at $Ra = 8000$, in accordance with the topology inferred from Figs. 6(d) and 7(d) for $Ra = 9000$.

Thermal field

The thermal field inside the cavity at $Ra = 4000$ and at $Ra = 9000$ is visualized in Figs. 9 and 10, respectively, in terms of surfaces of constant temperature. The form of these isosurfaces indicates the mode of circulation. The temperature isosurfaces at $Ra = 4000$ exhibit a more intense two-dimensionality and strati-

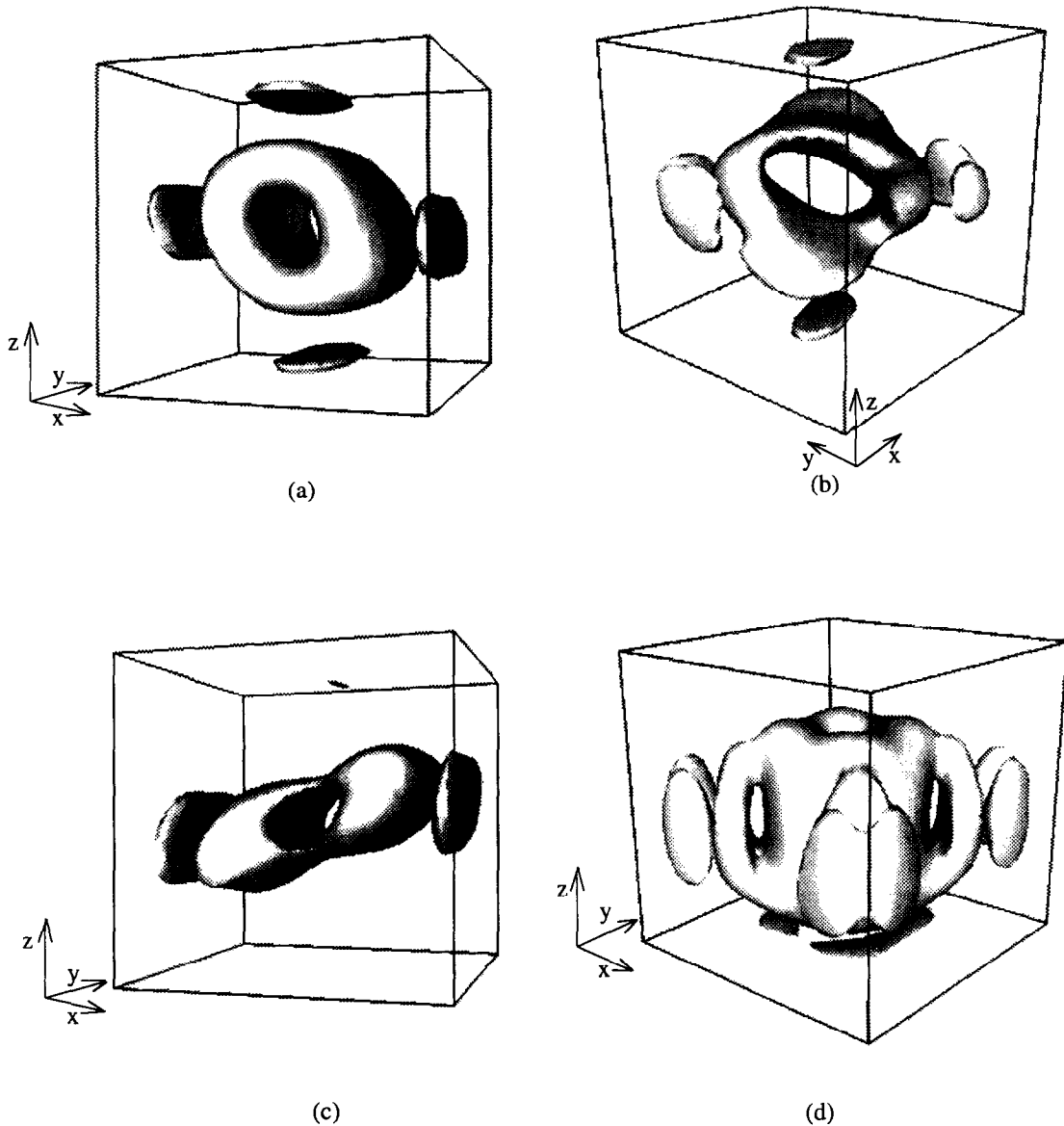


Fig. 7. Isosurfaces of the cross-product modulus at $Ra = 9000$ for the structures S1 (a) $H^* = 1100$; S2 (b) $H^* = 1100$; S3 (c) $H^* = 900$; S4 (d) $H^* = 120$.

fication than those corresponding to $Ra = 9000$, which, in turn, are more affected by the lateral walls. Figures 9(a) and (c) or 10(a) and (c) show that there are no obvious visual differences between the thermal fields corresponding to S1 and S3, whereas the flow patterns previously discussed for these structures reveal intrinsic structural differences between them. These results indicate that the thermal field is not a convenient way for visualizing the topology of flow structures in enclosures or near walls.

The effect of the type of structure on heat transfer rates at the top and bottom plates is shown in Fig. 11, where the 2D distribution of the local Nusselt number

is plotted for $Ra = 9000$. The 2D thermal fields are given in terms of lines of constant local Nusselt numbers for the four flow structures S1–S4 identified. In these plots, a maximum absolute value of the Nusselt number corresponds to a region of impingement of an ascending or descending current, while relatively low absolute values correspond to regions of boundary layer flow for the fluid leaving the two plates. Figures 11(a)–(d) and 11(e)–(h) show, respectively, the distribution of local Nusselt numbers at the top and bottom plates for the four structures present in the flow. For S1, S2 and S3 [Figs. 11 (a)–(g)], the distributions of the hot and cold plates are perfectly

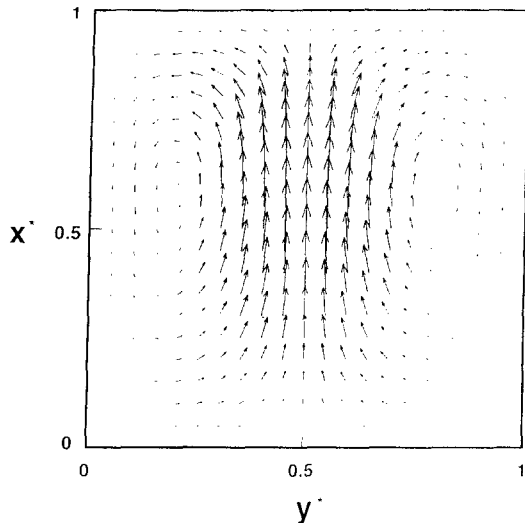


Fig. 8. Projection of the velocity vector field on the vertical plane $Z^* = 0.5$ at $Ra = 8000$ for the structure S4.

anti-symmetrical, in accordance with the presence of a single rotating roll. The maps for S4 agree with a nearly toroidal structure with dominating descending currents at the vertical edges and a strong ascending current in the core.

Although the distribution of local Nusselt numbers for S1 and S3 have a very similar appearance, a detailed study of Figs. 11(a) and (c), and 11(e) and (g), reveals a different heat transfer behaviour. Maximum heat transfer rates occur close to the vertical walls for S3 due to the elongation of this structure towards the two opposite horizontal edges parallel to the axis of rotation. This elongation provides extra space for flow circulation causing a decrease in recirculating velocities and yielding slightly lower values for the Nusselt numbers. The maps for S2 reveal that the orientation of the structure along the diagonal plane produces higher heat transfer rates, but in a narrower region than for the other two single roll structures. Among all different structures, S4 is by far the less effective for transferring heat between the top and bottom plates, as indicated by the lower values of the local Nusselt numbers given in Figs. 11(d) and (h).

Table 3 indicates the location (x^*, y^*) where the maximum values of the Nusselt number occur at the hot plate, for the four structures S1–S4. While at $Ra = 4000$ only S1 and S2 have different locations for the maximum heat transfer rates, at $Ra = 9000$ the location of the maximum value for S3 also separates from that of S1, getting closer to the lateral wall. Maximum values are centered somewhere in the diagonal for S2 and located near the center of the plate for S4, in accordance with the data of Figs. 11(a)–(d).

Surface averaged Nusselt numbers depend both on

the Rayleigh number and on the kind of structure present in the flow, as shown in Fig. 12. The variation of the averaged Nusselt number with Rayleigh number for structures S1–S3 is clearly different from that corresponding to S4. The same critical Rayleigh number, of approximately 3500 is observed for the first three structures (S1–S3), while the critical value for S4 occurs at around 7700, indicating two different bifurcations of the Navier–Stokes equations. The higher critical value for S4 suggests that this structure is more influenced by the lateral adiabatic walls.

The three single roll structures S1–S3 yield similar heat transfer characteristics, with Nusselt numbers increasing with a power of the Rayleigh number in the range 0.7–0.4. Figure 12 shows that S1 is the most efficient for transferring heat followed by S2, which is 2% less efficient, and by S3. It is interesting to note that while S3 is topologically similar to S1, it yields even lower heat transfer rates than S2, with a 4% drop at $Ra = 4000$ and a 7% at $Ra = 10000$. The variation of the Nusselt number with the Rayleigh number for S4 is similar to that for the single roll structures, but with transfer rates 65% lower.

CONCLUDING REMARKS

This numerical study presents a detailed description of the topology of the different convective structures present in a cubical cavity heated below, in the range $3500 \leq Ra \leq 10000$, using air ($Pr = 0.71$) as working fluid. It is interesting to note the ability of the second invariant of the velocity gradient tensor Π and the modulus of the vector product H to portray the structural characteristics of the flow. While Π gives closed surfaces that illustrate the structure characteristics, the 3D maps for H describe the fluid venae. The spatial distributions of the four stable detected structures are influenced by the four adiabatic lateral walls which favour certain privileged orientations. Two structures, S1 and S3, have orientations parallel to two opposite lateral walls while the other two, S2 and S4, are oriented along the diagonal of the top and bottom plates. The difference on the critical Rayleigh number for the single roll structures (S1, S2 and S3), $Ra_c = 3500$, and for the toroidal structure S4, $Ra_c = 7700$, suggests that there are different bifurcations of the Navier–Stokes equations. Moreover, the existence of four different structures makes the surface averaged Nusselt number dependent on the pattern adopted by the flow. The three single roll structures S1–S3 yield heat transfer rates at the top and the bottom plates that are 65% higher than those of the toroidal roll S4. All the structures are stable and do not evolve into other possible structures in the range $3500 \leq Ra \leq 10000$.

Acknowledgements The financial support received from DGICYT, project PB93-0656-C02-01, is gratefully acknowledged.

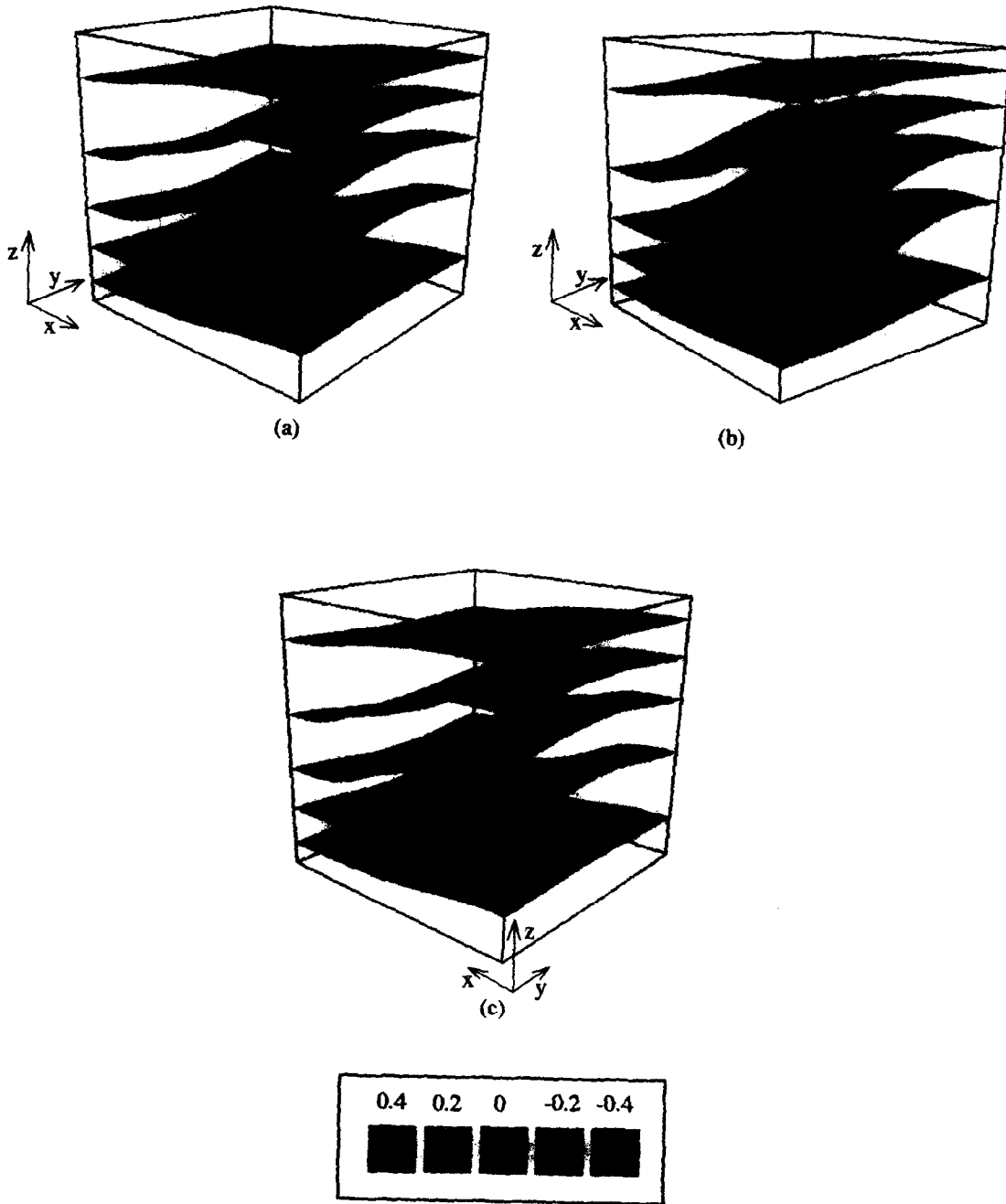


Fig. 9. Isosurfaces temperature at $Ra = 4000$ for the structures S1 (a); S2 (b); S3 (c).

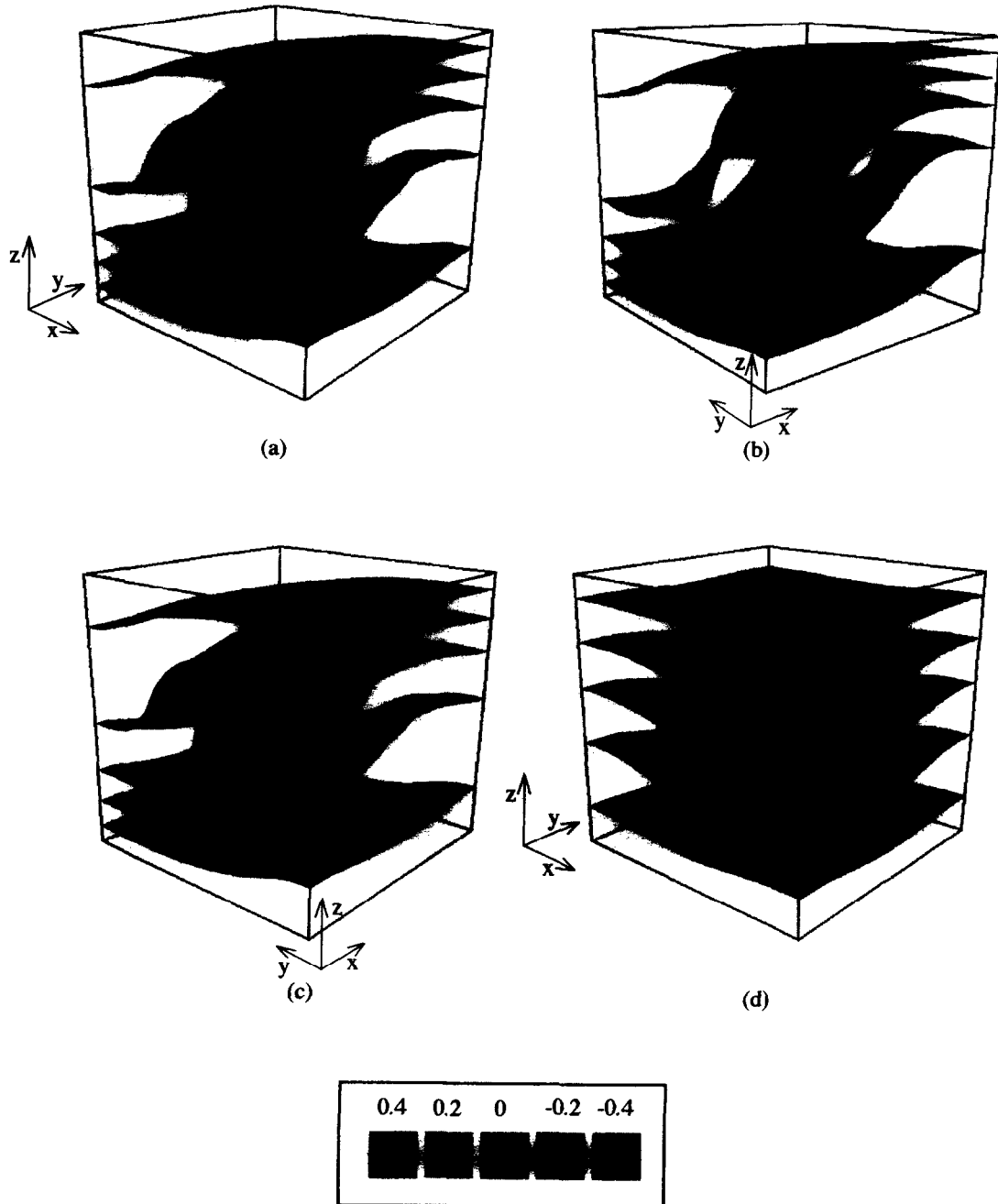


Fig. 10. Isosurfaces of temperature at $Ra = 9000$ for the structures S1 (a); S2 (b); S3 (c); S4 (d).

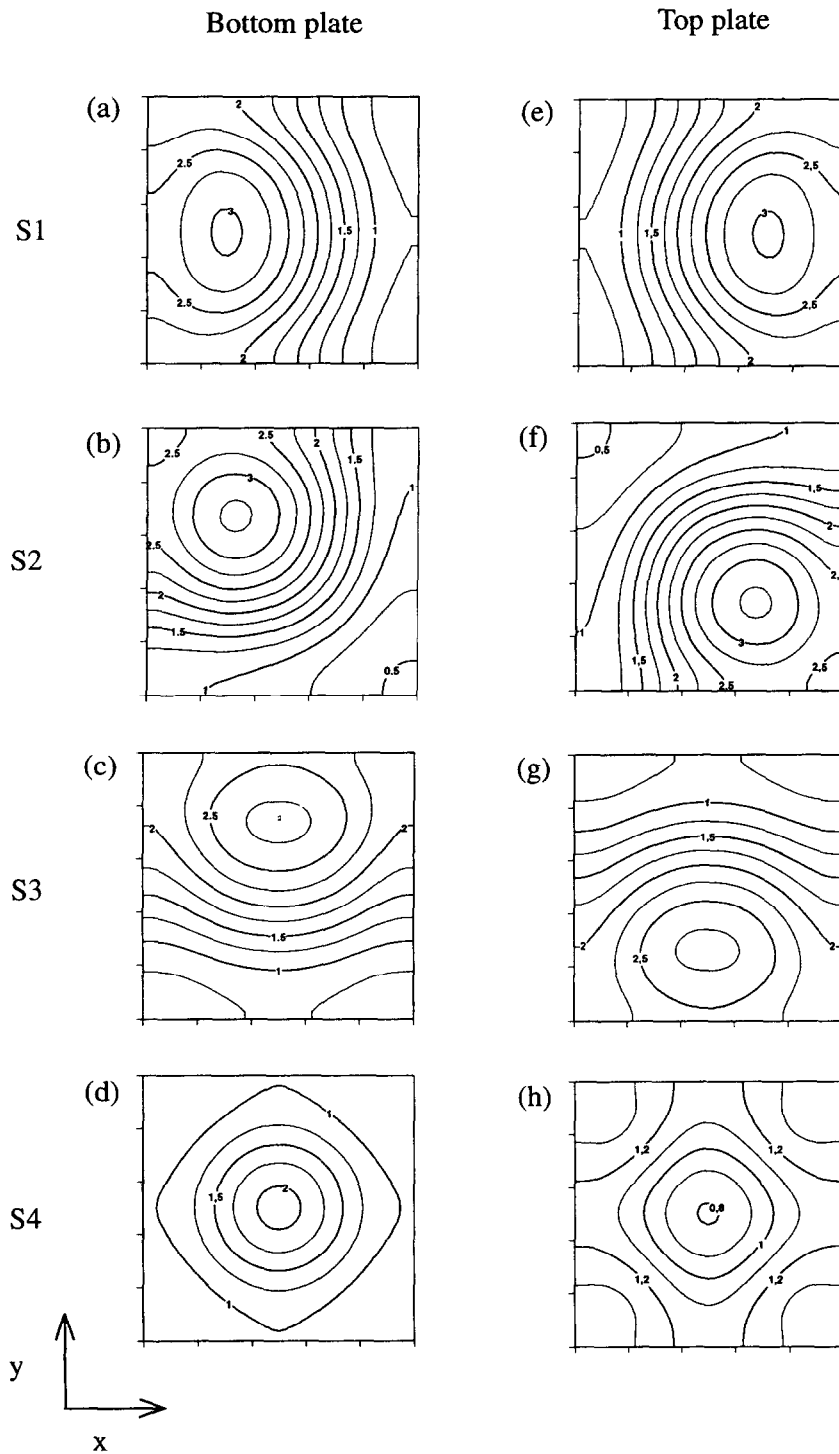


Fig. 11. Distribution of local Nusselt number at the bottom plate (a), (b), (c) and (d) and top plate (e), (f), (g) and (h) at $Ra = 9000$ for the structures S1 (a) and (e); S2 (b) and (f); S3 (c) and (g); S4 (d) and (h).

Table 3. Position of the maximum values of local Nusselt number at the bottom plate

Ra	S1		S2		S3		S4	
	x^*	y^*	x^*	y^*	x^*	y^*	x^*	y^*
4000	0.20	0.50	0.27	0.73	0.50	0.80	-	-
9000	0.30	0.50	0.32	0.68	0.50	0.75	0.50	0.50

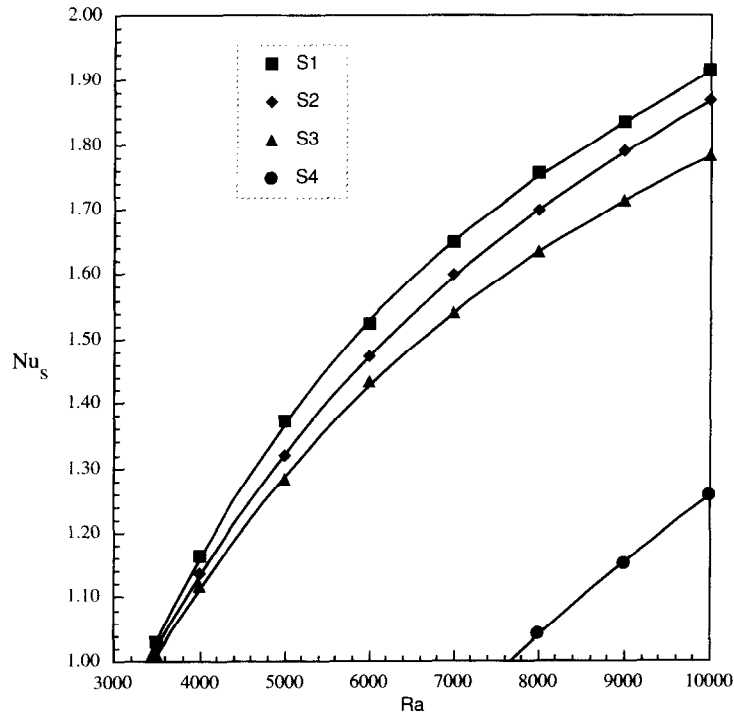


Fig. 12. Variation of the surface averaged Nusselt number with Rayleigh number for the four convective structures S1–S4.

REFERENCES

1. E. Koschmieder, *Bénard Cells and Taylor Vortices*. Cambridge Monographs on Mechanics and Applied Mathematics. Cambridge University Press, Cambridge, U.K. (1993).
2. M. H. Bénard, Les tourbillons cellulaires dans une nappe liquide transportant de la chaleur par convection en régime permanent, *Ann. Chim. Phys.* **23**, 62–144 (1901).
3. Rayleigh (Lord), On convection currents in a horizontal layer of fluid when the higher temperature is on the under side, *Philos. Mag.* **32**, 529–546 (1916).
4. E. L. Koschmieder, Bénard convection, *Adv. Chem. Phys.* **26**, 177–212 (1974).
5. C. Normand, P. Yves and M. G. Velarde, Convective instability: a physicist's approach, *Rev. Mod. Phys.* **49**, 581–624 (1977).
6. H. Oertel, Thermal instabilities. In *Convective Transport and Instability Phenomena* (Edited by J. Zierep and H. Oertel), pp. 3–24. G. Braun, Karlsruhe (1982).
7. S. Ostrach, Natural convection in enclosures, *J. Heat Transfer* **110**, 1175–1190 (1988).
8. K. T. Yang, Transitions and bifurcations in laminar buoyant flows in confined enclosures, *J. Heat Transfer* **110**, 1191–1203 (1988).
9. I. Catton, The effect of insulating vertical walls on the onset of motion in a fluid heated from below, *Int. J. Heat Mass Transfer* **15**, 665–672 (1972).
10. W. L. Heitz and J. W. Westwater, Critical Rayleigh numbers for natural convection of water confined in square cells with L/D from 0.5 to 8, *J. Heat Transfer* **93**, 188–196 (1971).
11. S. H. Davis, Convection in a box: linear theory, *J. Fluid Mech.* **30**, 465–478 (1967).
12. K. Stork and U. Müller, Convection in boxes: experiments, *J. Fluid Mech.* **54**, 599–611 (1972).
13. H. Ozoe, K. Yamamoto, S. W. Churchill and H. Sayama, Three-dimensional, numerical analysis of laminar natural convection in a confined fluid heated from below, *J. Heat Transfer* **98**, 202–207 (1976).
14. R. Hernández and R. L. Frederick, Spatial and thermal features of three-dimensional Rayleigh–Bénard convection, *Int. J. Heat Mass Transfer* **37**, 411–424 (1994).
15. D. D. Gray and A. Giorgini, The validity of the Boussinesq approximation for liquids and gases, *Int. J. Heat Mass Transfer* **19**, 545–551 (1976).
16. I. Cuesta, Estudi numèric de fluxos laminars i turbulents en una cavitat cúbica, Ph. D. Thesis, Universitat Rovira i Virgili, Tarragona, Spain (1993).
17. I. Cuesta, F. X. Grau and F. Giralt, Simulació numèrica de fluxos 3D no estacionaris mediante el código de segundo orden 3DINAMICS, *Anales de Química* (submitted).
18. S. V. Patankar, *Numerical Heat Transfer and Fluid Flow*. Series in Comparative Methods in Mechanical and Term. Sciences. McGraw-Hill, New York (1980).
19. B. P. Leonard, A stable and accurate convective modelling procedure based on quadratic upstream interpolation, *Comp. Meth. Appl. Mech. Engng* **19**, 59–88 (1979).

20. CH-Y. Perng and R. L. Street, Three-dimensional unsteady flow simulations: alternative strategies for a volume-averaged calculation, *Int. J. Numer. Meth. Fluids* **9**, 341–362 (1989).
21. A. A. Amsden and F. H. Harlow, The SMAC method: a numerical technique for calculating incompressible fluid flows, Los Alamos Scientific Laboratory of the University of California, LA-4370 (1970).
22. P. K. Koshla and S. G. Rubin, A conjugate gradient iterative method, *Comp. Fluids* **9**, 109–121 (1981).
23. D. W. Peaceman and H. H. Rachford, The numerical solution of parabolic and elliptic differential equations, *J. Soc. Ind. Appl. Math.* **3**, 28–41 (1955).
24. G. Grötzbach, Direct numerical simulation of laminar and turbulent Bénard convection, *J. Fluids Mech.* **19**, 27–53 (1982).
25. T. Fusegi, J. M. Hyun, K. Kuwahara and B. Farouk, A numerical study of three-dimensional natural convection in a differentially heated cubical enclosure, *Int. J. Heat Mass Transfer* **34**, 1543–1557 (1991).
26. P. Haldenwang, Résolution tridimensionnelle des équations de Navier–Stokes par méthodes spectrales Tcheycheff: application à la convection naturelle, Ph. D. Thesis, Université de Provence (1984).
27. S. Ben Mabrouk, Etude numérique de la convection naturelle en cavité tridimensionnelle, Ph. D. Thesis, Université de Poitiers (1984).
28. G. De Vahl Davis and I. P. Jones, Natural convection in a square cavity: a comparison exercise, *Int. J. Numer. Meth. Fluids* **3**, 227–248 (1983).
29. M. P. Arroyo and J. M. Savirón, Rayleigh–Bénard convection in a small box: spatial features and thermal dependence of the velocity field, *J. Fluid Mech.* **235**, 325–348 (1992).
30. J. J. Van Wijk, A. J. S. Hin, W. C. de Leeuw and F. H. Post, Three ways to show 3D fluid flow, *IEEE Comput. Graphics Appl.* **14** Sept. (1994).
31. J. C. R. Hunt, A. A. Wray and P. Moin, Eddies, streams and convergence zones in turbulent flows, *Proceedings of the 1988 Summer Program*, NASA—Stanford Center for Turbulence Research, 193–208 (1988).
32. N. D. Sandham and L. Kleiser, The late stages of transition to turbulence in channel flow, *J. Fluid Mech.* **245**, 319–348 (1992).
33. F. Hussain, New approaches to vortex dynamics: core dynamics, helical waves, and interaction with fine scale turbulence. In *Eddy Structure Identification in Free Turbulent Shear Flows* (Edited by J. P. Bonnet and M. N. Glauser), pp. 13–25 (1993).
34. S. Shirayama, Processing of computed vector fields for visualization, *J. Comp. Phys.* **106**, 30–41 (1993).